

# PROPERTIES AND EVOLUTION OF THE EARTH'S CORE AND GEODYNAMO

F. Nimmo<sup>1</sup> and D. Alfe<sup>2,3</sup>

<sup>1</sup> Dept. Earth Sciences, University of California Santa Cruz, CA 95064, USA (fnimmo@es.ucsc.edu)

<sup>2</sup> Dept. Physics & Astronomy, University College London, WC1E 6BT, UK (d.alfe@ucl.ac.uk)

<sup>3</sup> INFM DEMOCRITOS, National Simulation Centre, via Beirut 2-4, 34125, Trieste, Italy

## Abstract

We review recent advances in the study of the Earth's iron core, focusing on three areas: the properties of the core-forming materials, the manner in which core motions generate the Earth's magnetic field (the dynamo), and the evolution of both the core and the dynamo. Ab initio computer simulations of the behaviour of iron alloys under core conditions suggest that the inner (solid) and outer (liquid) core contain 8% sulphur/silicon, and 8-10% sulphur/silicon plus 8-13% oxygen, respectively. The inner core boundary for these materials is at  $\sim$ 5500 K. Although computer simulations of the dynamo lack sufficient resolution to match likely terrestrial parameter values, such models can now reproduce the spatial and temporal behaviour of the observed magnetic field. The present-day dynamo occurs because the mantle is extracting heat (at a rate of  $9 \pm 3$  TW); the resulting inner core growth drives core convection and implies a young inner core age ( $<1.5$  Gyr). A long-lived dynamo requires rapid core cooling, which tends to result in an inner core larger than that observed. A possible solution to this paradox is that radioactive potassium may reside in the core. We also briefly review the current state of knowledge for cores and dynamos in other planetary bodies.

## 1. Introduction

The rocky exterior of the Earth conceals a Mars-sized iron body at its centre: the core. The core is of fundamental importance to the thermal and magnetic behaviour of the Earth as a whole. Recent advances in computational power and experimental techniques have galvanized the study of the core in at least three areas: the properties of the core-forming materials; the manner in which core motions generate the Earth's magnetic field (the geodynamo); and the evolution of both the core and the geodynamo through time. In this review we focus on these three issues.

We begin with a description of the Earth's interior structure, and how it is deduced. We also describe the main characteristics of the Earth's magnetic field, and how it has varied in time. These preliminaries completed, in Section 3 we examine how recent results have helped to pin down the composition and temperature structure of the core. In Section 4 we discuss the progress made

in numerical models, which can now reproduce many aspects of the geodynamo. In Section 5 we discuss how the energy balance of the present-day core maintains the dynamo, and speculate how this energy balance may have changed over the course of Earth's history. We conclude with a look at the cores and dynamos of other Earth-like bodies in this solar system, and suggest likely directions of research for the next decade.

## 2. The Interior Structure of the Earth

With the exception of the Earth, our knowledge of the internal structure of silicate (rocky) planets is rather limited. Our knowledge of the Earth's structure is much more complete, thanks to the study of earthquakes (see below). However, even in the absence of this kind of information, there are several lines of evidence suggesting that silicate planets should possess a mostly iron core.

Firstly, the raw material of the solar system had a composition which was probably similar to that of the Sun and a common class of meteorites, the chondrites. The ratio of silicon to iron in these materials is roughly 1:1 by volume (Lodders and Fegley 1998); since neither element is particularly volatile, the Earth, and other similar bodies, should have retained their full complement. While some of the iron is likely to have been bound up in silicate minerals, in the absence of any other evidence one would expect the terrestrial planets to consist of silica-rich and iron-rich zones. The multiple collisions which gave rise to the terrestrial planets will have led to hot, and possibly molten, starting conditions (Tonks and Melosh 1993); under these conditions, the dense iron-rich material will have migrated to the centre, forming an iron core (Stevenson 1990).

This rather theoretical argument is supported by observations. For instance, the near-surface of the Earth consists of a silicate mantle with a density of around  $3300 \text{ kg m}^{-3}$ . This density is considerably less than the mean density of the planet ( $5500 \text{ kg m}^{-3}$ ). Even though the mantle density would increase with depth, due to the compressibility of rock, the likely increase is insufficient to account for the observed density. Thus, the presence of a subsurface, high density zone is required, and the compositional arguments outlined above imply that the dense material is primarily iron.

Further evidence comes from the moment of inertia of the Earth, which is accurately known from measurements of satellite orbits and the rate of precession of the rotation axis, and which constrains the distribution of mass within the Earth. A uniform sphere has a normalized moment of inertia of 0.4; the Earth's value of 0.3307 indicates that the mass is concentrated towards the centre of the planet. For a simple two-layer (core plus mantle) planet, the core radius can be determined if the densities of the two layers are known. Table 1 gives the densities and moments of inertia of several silicate bodies; these data and the arguments above strongly suggest that iron cores are a common planetary feature.

Table 1: Geophysical parameters of silicate planetary bodies. Data are from Lodders and Fegley (1998), except as indicated otherwise.  $R_c$  is the core radius,  $C$  is the polar moment of inertia.  $m$  is the magnetic dipole moment of the body, measured in Tesla  $\times R^3$ , and indicates the strength of the magnetic field. <sup>a</sup> Khan et al. (2004) <sup>b</sup> Schubert et al. (1988) <sup>c</sup>Konopliv and Yoder (1996) <sup>d</sup> Yoder et al. (2003) <sup>e</sup> Anderson et al. (1996).

	Earth	Moon	Mercury	Venus	Mars	Ganymede
radius $R$ (km)	6371	1737	2438	6052	3390	2634
mass $M$ ( $10^{24}$ kg)	5.97	0.07	0.33	4.87	0.64	0.15
bulk density (kg m $^{-3}$ )	5515	3344	5430	5243	3934	1940
surface gravity $g$ (m s $^{-2}$ )	9.8	1.6	3.7	8.9	3.7	1.4
$C/MR^2$	0.3307	0.394	-	-	0.366	0.31
$R_c/R$	0.55	0.2 <sup>a</sup>	0.75 <sup>b</sup>	0.5 <sup>c</sup>	0.45-0.55 <sup>d</sup>	0.15-0.5 <sup>e</sup>
$m(\times 10^4)$	0.61	-	0.003	-	-	0.008

Perhaps surprisingly, we can also differentiate between a liquid and a solid core. The solid Earth deforms under the gravitational attraction of the Sun and the Moon, that is, it has tides. These tides are much smaller in amplitude (typically 0.2 m) than the tides associated with the oceans, but are still measurable. The deformation depends on the rigidity of the interior (Murray and Dermott 1999). Predicted tidal amplitudes, assuming a uniform (seismologically inferred) mantle rigidity, were too small; one solution to the problem was to postulate that the core had negligible rigidity, that is, it was fluid (Jeffreys 1929).

Similar arguments can be applied to bodies other than the Earth. For instance, tidal deformation studies suggest that the cores of Mars (Yoder et al. 2003), the Moon (Williams et al. 2001), Venus (Konopliv and Yoder 1996) and Mercury (Margot et al. 2004) are at least partially liquid. We will return to the cores of the other planets later in this article, but for now we will focus on that of the Earth, since we understand it in so much more detail.

Fig. 1a shows a schematic cross-section of the Earth. The outer half of the planet consists of a silicate mantle. The near-surface is made up of rigid tectonic plates, roughly 100 km thick, which move laterally and are eventually recycled into the mantle at subduction zones. At a depth of 2920 km the mantle gives way to the liquid outer core; this interface is known as the core-mantle boundary (CMB). The liquid outer core in turn gives way to a solid inner core at a depth of 5180 km, the inner core boundary (ICB). The outer core is probably well-mixed and relatively homogeneous; however, both the inner core and the mantle are likely to be laterally heterogeneous. A particularly complex region is the base of the mantle, which forms a hot boundary layer from which convective

plumes rise.

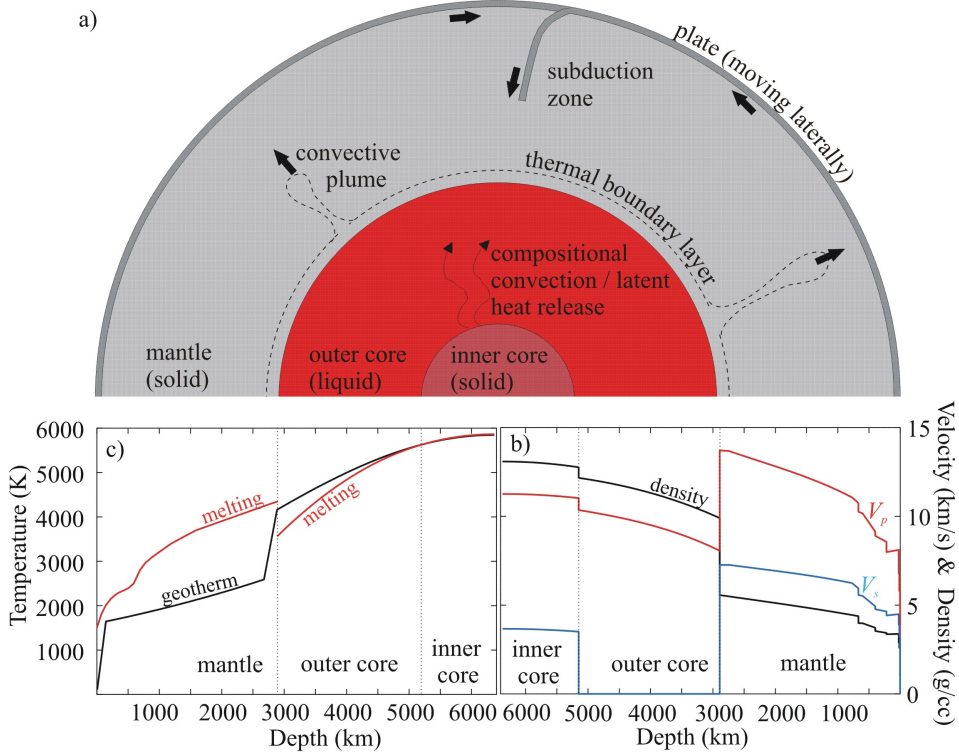


Figure 1: a) Schematic cross-section of the Earth. Boundary layer thicknesses are to scale. b) Variation in P-wave ( $V_p$ ) and S-wave ( $V_s$ ) velocities and density with depth. From Dziewonski and Anderson (1981). c) Variation in temperature and melting curve (solidus) with depth. Mantle melting curve from Boehler (2000); other curves from Nimmo et al. (2004).

The remarkable detail in which the interior structure of the Earth is known is thanks almost entirely to seismology, the study of earthquakes (see Stein and Wysession 2000 for a comprehensive overview). Earthquakes occur because of the relative motions of the Earth's different tectonic plates, and generate waves which propagate through the Earth. An earthquake caused by fault slip of about 1 m or more is easily detectable with modern seismometers on the other side of the globe; about 50 such earthquakes occur each year. Seismometers at different locations will detect seismic waves whose paths have sampled different parts of the Earth's interior; since the seismic velocity varies with depth, the relative wave arrival times at different seismometers can be used to infer the velocity structure of the Earth. The outermost core, having a slower velocity than the overlying mantle, refracts the waves so as to leave a 'shadow zone' in which very few arrivals are observed. The existence of this shadow zone was the first seismological evidence for the core; later detection of arrivals within this zone confirmed the existence of an inner core.

Because the bulk of the interior of the Earth is solid, both transverse (S) and longitudinal (P) waves will propagate. The propagation velocities, which depend on the local density and elastic constants, are different. In particular, transverse waves do not propagate through liquids. This fact allowed identification of the outer core as a fluid: S waves cannot propagate directly through the outer core, and are therefore nearly absent at a characteristic range of angular distances from the earthquake source. Once both the P and S velocities are known as a function of radial distance, it is then possible to iteratively infer the variation in density and gravity with depth.

The very largest earthquakes set the whole Earth vibrating with periods of tens of minutes. The amplitudes and periods of the different oscillations depend on the velocity and density structure of the Earth, with shorter-wavelength oscillations being more sensitive to shallow structures and vice versa. Given enough oscillations, the density and velocity structures can be inverted for, and thus provide an independent check on the results obtained from seismic wave arrival times.

Results obtained by combining these two methods are shown in Figure 1b. The increase in velocity with depth is primarily due to the decrease in compressibility with increasing pressure. The S wave velocity drops to zero in the outer core because it is a fluid. The density increases with depth, as expected. It turns out that the density of the outer core is less than that expected for pure iron, suggesting the presence of a contaminant (see Section 3.4). The increase in density at the ICB, conversely, is larger than one would expect for a simple phase change, suggesting that the contaminant is not being incorporated into the solid core. This expulsion of a light constituent as the inner core solidifies provides a major source of energy to drive the dynamo (see Section 5.1).

Having established the radially-averaged structure of the Earth, it then becomes possible to look for lateral variations in seismic velocity, a process known as seismic tomography. Tomographic images now routinely detect both subducting plates and upwelling plumes (Montelli et al. 2004). Some of the velocity anomalies inferred, particularly those near the CMB, are too large to be caused simply by temperature changes, and may involve compositional or phase variations (Oganov and Ono 2004) or melting (Williams and Garnero 1996). Perhaps more surprisingly, the inner core also appears to contain structure: the outermost part is isotropic but of variable thickness, while the inner part has a fabric (Song 2003, Souriau and Poupinet 2003). This fabric is critical for observing inner core rotation (see Section 4).

## 2.1 Thermal Structure of the Earth

As described above, the density structure of the Earth can be inferred directly from seismology. Equally important, however, is the temperature structure of the Earth. Within the rigid surface plates, the temperature increases roughly linearly with depth, and heat is transported by conduction. Somewhere within the range 1200-1600 K, mantle material stops behaving in a rigid fashion and

starts to flow, so the base of the plate occurs within this temperature interval. The mantle below is sufficiently warm that it undergoes convection.

A packet of convecting mantle material moves sufficiently rapidly that it does not exchange appreciable heat with its surroundings. This so-called adiabatic situation means that, as the material rises and expands, it cools. Mantle material which rises all the way to the surface is sufficiently hot that it exceeds its melting temperature and generates a crust; the  $\sim 7$  km thickness of the resulting oceanic crust implies a mantle surface (or potential) temperature of about 1600 K (McKenzie and Bickle 1988).

The adiabatic effect depends on gravity, thermal expansivity and heat capacity, all of which are reasonably well known. The resulting adiabatic gradient is about 0.5 K/km (Fig 1c); this gradient is shallower than the conductive gradient in the near-surface because heat is being transported by convection, not conduction. Following the adiabatic gradient (which decreases a little with depth), the temperature near the base of the mantle is about 2700 K. However, there will exist a boundary layer at the base of the mantle across which the temperature increases rapidly to that at the outer edge of the core.

The temperature at the ICB is (by definition) the core melting temperature at that pressure. Because the outer core is convecting, it will also have an adiabatic temperature gradient (of about 0.8 K/km). Thus, if the temperature at the ICB is known, the temperature everywhere in the outer core is also determined. This is why it is so important to determine the melting behaviour of iron: it provides a tie point from which temperatures elsewhere can be calculated.

Despite a great deal of experimental and theoretical effort in determining the melting temperature of iron at core conditions, only in the last few years have the uncertainties been reduced to even moderately acceptable levels. We will discuss recent progress in this field in Section 3 below; here, we will simply point out the example temperature structure shown in Fig. 1c. It shows the conductive plate at the surface, the adiabatic gradient within the mantle, and the boundary layer at the base of the mantle. The location of the inner core is determined by the intersection of the adiabat with the melting curve. The adiabatic temperature drop across the liquid outer core is 1450 K, the ICB is at 5600 K, and the CMB is 4150 K. The uncertainties associated with some of these numbers are still large (see Section 3); however, the basic picture is certainly correct.

## 2.2 Magnetic Observations of the Earth

The present-day magnetic field of the Earth is well characterized. As recognized by William Gilbert in 1600, it resembles that of a bar magnet, with north and south poles (dipolar). The dipole axis is currently inclined at about  $10^\circ$  to the rotation axis. At short wavelengths ( $< 1000$  km) the surface magnetic field is dominated by crustal anomalies, but the longer wavelength features are due

to processes occurring within the core. Short wavelength features are also undoubtedly generated within the core, but are not visible at the surface because they are strongly attenuated with radial distance. A further complication is that the so-called toroidal component of the core's magnetic field has field lines which are parallel to the surface of the core, and are thus unobservable at the Earth's surface. Thus, the field that we can measure at the surface is different in both frequency content and amplitude from the field within the core.

The behaviour of the Earth's magnetic field over time is of great interest (see reviews by Valet 2003 and Jacobs 1998). Modern measurements of the variation in intensity and orientation of the field date back only 150 years, to the time of Gauss. Less precise observations, mostly from naval expeditions, extend the historical record back to roughly 1500 A.D., and well-dated archaeological data cover the last  $\sim$ 10 kyr. Prior to this time, observations of field orientation and intensity rely on the natural (remanent) magnetisation of either volcanic rocks or sediments. The former are problematic because high-resolution dating is difficult to achieve; dating the latter is easier, but the processes by which sediments acquire magnetic characteristics are not well understood, and may involve complicating effects such as changes in ocean chemistry.

Despite the difficulties, several time-dependent characteristics of the field are evident. Firstly, over the last four centuries, the tilt and the amplitude of the dipolar field have changed by tens of percent (Barton 1989). Over the same timescale, several features of the field appear to have drifted westwards with time, at a rate of about  $0.5^\circ$  per year. Secondly, over timescales  $>$  a few thousand years the mean position of the magnetic axis coincides with the rotation axis (Valet 2003). Thirdly, the field appears to have remained predominantly dipolar over time (though see Bloxham 2000), and has apparently persisted for at least 3500 Myrs (McElhinny and Senanayake 1980), with the maximum field intensity having exceeded the present day value by no more than a factor of five (Valet 2003, Dunlop and Yu 2004). Fourthly, and much the most important, the polarity of the magnetic axis undergoes irregular reversals. Recent reversals have occurred roughly every 200 kyr, and take place rapidly (about 7 kyr (Clement 2004)). However, there is a wide scatter in reversal frequency; for instance, there were no reversals at all in the period 125-85 Ma. The earliest reversal identified to date occurred at 3214 Ma (Layer et al. 1996). Incomplete reversals, or excursions, appear to take place more frequently. Finally, it is argued that the path swept out by the magnetic poles during reversals may be preferentially concentrated around the Pacific (Laj et al. 1991), though this is controversial (Prevot and Camps 1993, Love 2000). These observations provide constraints on the models for magnetic field generation, to be discussed below.

### 3. Core Properties

As discussed above, inferring the thermal structure of the core requires a knowledge of the

melting temperatures of iron and iron alloys at core pressures. Similarly, understanding how light impurities partition between the solid and liquid core phases is necessary to infer the core composition. The traditional way of answering these questions is by experiments, in which the high pressures may be either static (e.g. diamond anvil cells) or transient (shock waves). Carrying out such experiments is exceedingly challenging, and typically results in melting temperature uncertainties of  $\pm 500$  K. More recently, computational methods based on quantum mechanics have been used to predict the behaviour of iron and iron alloys at core conditions. Here we will focus on the computational approach, and in particular that of the group based at UCL. As discussed below, several other groups have obtained similar results using slightly different approaches (Laio et al. 2000, Belonoshko et al. 2000).

The basic approach of the computational methods is to calculate the chemical potential of the material at the conditions of interest. This approach relies on the fact that the minimum of the chemical potential defines the stability. Thus, for example in the context of melting, at a temperature above the melting temperature the chemical potential of the liquid will be lower than that of the solid, and conversely at a temperature below the melting temperature the chemical potential of the solid is lower. It follows that at the equilibrium between two phases (e.g. solid and liquid at the melting temperature) the chemical potentials of the two phases are equal. These chemical potentials can be calculated, and therefore the melting curve can be determined.

Analogously, in a mixture of elements A and X, equilibrium between solid and liquid implies the continuity of the chemical potentials of *both* A and X across the phase boundary. The equality of the chemical potentials of A and X in the solid and in the liquid determines the partitioning of A and X between solid and liquid. This information can be used to infer the composition of the Earth's core, as explained below.

In what follows we will first briefly describe the theoretical framework on which the calculations were based, and then present the results for the melting curve of iron, and the partitioning of light elements in the core.

### 3.1 First principles calculations

With *first principles simulations* one usually means calculations in which no adjustable parameter and no experimental input is allowed (apart from some fundamental constants, such as the charge on the electron and the Planck constant). In the context of simulating the properties of matter, this means solving the Schrödinger equation  $\mathcal{H}\Psi_N = \mathcal{E}\Psi_N$ , where  $\mathcal{H} = \mathcal{T} + \mathcal{V}$  is the *Hamiltonian* of the system which contains  $N$  particles (both electrons and nuclei), with  $\mathcal{T}$  the kinetic energy and  $\mathcal{V}$  the potential energy,  $\mathcal{E}$  the energy of the system, and  $\Psi_N$  the many-body *wavefunction*, which is a complicated function of the positions of the  $N$  particles in the system. Since the electrons are at

least three order of magnitudes lighter than the nuclei, it is customary to introduce the so called *adiabatic approximation*, in which the motion of the electrons is decoupled from the motion of the nuclei. This in practice means solving a new Schrödinger equation  $\mathcal{H}\{R\}\Psi_n\{R\} = \mathcal{E}\{R\}\Psi_n\{R\}$ , where now the Hamiltonian is only a function of the  $n$  electronic degrees of freedom, and depends parametrically on the nuclear degrees of freedom  $\{R\}$ . The energy  $\mathcal{E}\{R\}$  is interpreted as a potential energy for the motion of the nuclei. From this, one can calculate the forces on the nuclei, which, for example, can be used to integrate the Newton's equation of motion and perform *molecular dynamics* simulations.

Even with this simplification though, the problem of solving the modified Schrödinger equation remained very difficult, at least until the introduction of a reformulation of quantum mechanics in the mid 60's, named *Density Functional Theory* (DFT). DFT was a breakthrough in the state of the art of quantum mechanics, made in 1964 by Hohenberg and Kohn (Hohenberg and Kohn 1964, Kohn and Sham 1965). In this section we review only main points of the theory; for a rigorous description the reader should consult the original papers or, for example, the excellent books of Parr and Wang (Parr and Wang 1989) or Dreizler and Gross (Dreizler and Gross 1990).

The central idea of DFT is that the complicated many-body wavefunction  $\Psi_n$  is not needed, and the important physical quantity is the electronic charge  $\rho(r)$ , which is only a function of the three-dimensional variable  $r$ . The energy of the system is a *functional* of the density, and can be written as  $\mathcal{E}[\rho] = \mathcal{F}[\rho] + \mathcal{V}[\rho]$ , where  $\mathcal{V}[\rho]$  is the potential energy of the electronic charge density  $\rho$  in the external potential  $\mathcal{V}$  (e.g. the potential due to the nuclei), and  $\mathcal{F}[\rho]$  a *universal functional* of  $\rho$ . The ground state energy of the system is given by the minimum of  $\mathcal{E}[\rho]$  with respect to  $\rho$ , and the electronic charge density which minimises the total energy is the ground state electronic charge density.

Of course, it rarely happens that a simple reformulation of a problem solves all the difficulties, and indeed this is not the case for DFT: the functional  $\mathcal{F}[\rho]$  is unknown. However, Kohn and Sham proposed (Kohn and Sham 1965) a simple approximation called the *local density approximation* (LDA), which made it possible to define an approximated  $\mathcal{F}[\rho]$ . Although the LDA was constructed to work for homogeneous systems, this approximation turned out to also work amazingly well for highly inhomogeneous systems like molecules and surfaces, and it is probably fair to say that DFT owes its tremendous success in the past forty years to this approximation. Recently, more sophisticated approximations have been proposed, like the so called *generalised gradient corrections* (GGA) (e.g. Wang and Perdew 1991, Perdew et al. 1996), but the LDA is still playing a major role in the DFT community.

An additional approximation which contributed to the great success of DFT was the so called

*pseudo-potential* approximation (e.g. Bachelet et al. 1982). The main point here is the recognition that only the outermost electrons of the atoms are involved in bonding, the so called *valence* electrons. This means that the *core* electrons which are tightly bound to the nuclei can be treated as frozen in their atomic configurations, and included only implicitly in the calculations. This is done by replacing the potential generated by the bare nuclei, with a *pseudo-potential* generated by the ionic cores, which are formed by the nuclei surrounded by the frozen core electrons. The quality of this approximation can be easily tested by explicitly including more electrons in *valence*.

The increasing popularity of DFT in the physical, chemical, and more recently geological and biological community, is due to its exceptional reliability in reproducing experimental results, giving DFT-based methods unparalleled predictive power. The success of these kinds of first principles calculations is also due to the increasingly widespread availability of large computational resources, as well as to more and more efficient computer codes.

In the next section we briefly describe the main points relevant to the calculations of chemical potentials from first principles, and we report the results for the melting curve of iron and the partitioning of light elements in the core in the following two sections.

### 3.2 Free energies

Chemical potentials are closely related to *free energies*. In particular, in a one component system the chemical potential  $\mu$  is given by the Gibbs free energy per molecule,  $\mu = G/N = F/N + pV/N$ , where  $F$  is the Helmholtz free energy of the system containing  $N$  particles,  $p = -\partial F/\partial V|_T$  is the pressure and  $V$  is the total volume.

To calculate  $F$  at a given state  $(V, T)$ , it is possible to use the technique known as *thermodynamic integration* (see e.g. Frenkel and Smit 1996). This is a general scheme to compute the free energy difference  $F - F_0$  between two systems, whose potential energies are  $U$  and  $U_0$  respectively. The idea is that  $F$  is the “difficult” free energy of the quantum mechanics system, and  $F_0$  the free energy of a system where the interactions between the atoms are approximated by some simple relation.

The free energy difference  $F - F_0$  is the reversible work done when the potential energy function  $U_0$  is continuously and reversibly switched to  $U$ . This switching does not correspond to a physical process, but it is a well defined mathematical procedure which can be carried out in a computer. The computational effort is proportional to the “distance” between the reference and the quantum mechanical systems. Therefore, the crucial point here is that the reference system should be chosen to be as close as possible to the quantum mechanics system, because this minimises the number of quantum mechanics calculations needed. To calculate the free energy of the reference system  $F_0$  one can use the same procedure, and evaluate  $F_0 - F^*$ , where  $F^*$  is the free energy of some other simple reference system whose free energy is known. Here, since the calculations do not involve

heavy quantum mechanics calculations, one can afford “large distances” between these two systems, and possibly  $F^*$  could even be the free energy of a perfect gas (i.e. a system with no interactions between the particles).

To compute the melting temperature of iron, we performed calculations at a number of thermodynamic states spanning the conditions of the Earth’s core, and the calculated Helmholtz free energies  $F(V, T)$  were fitted to polynomials in volume and temperature. From this it is possible to obtain all the relevant thermodynamical properties by appropriate differentiation of  $F$ .

Similar techniques can be used to evaluate the chemical potentials of the elements of a mixture. For example, the chemical potential  $\mu_X$  of an element  $X$  in a solution  $A/X$  (we may identify element  $A$  with the solvent and  $X$  with the solute, but the description is completely general) is equal to the change of Helmholtz free energy of the system as one atom of the element  $X$  is added to the system at constant volume and constant temperature. This change of free energy can be evaluated using the techniques of thermodynamic integration described above. A detailed explanation of how this is done can be found in Alfè et al. 2002a. We shall see below how the ability of calculating the chemical potentials of the elements in a solution can be used in conjunction with seismological data to put constraints on the composition of the core.

### 3.3 The melting curve of iron

To determine the melting curve of iron we calculated the chemical potential  $\mu$  of pure iron as a function of pressure and temperature for both solid and liquid (Alfè et al. 1999, Alfè et al. 2001, Alfè et al. 2002b). In a one component system this is the same as the Gibbs free energy per atom  $G/N$ . In fact, we calculated the Helmholtz free energy  $F$  as a function of volume and temperature and then we obtained  $G$  from its usual relation  $G = F + pV$ . As mentioned above, for any fixed pressure the continuity of  $G$  with respect to temperature defines the melting transition, which is found by the point where the Gibbs free energies of liquid and solid become equal,  $G_l(p, T_m) = G_s(p, T_m)$ .

Figure 2 shows the melting curve of iron from pressures of 50 to 400 GPa. The solid black line is the result obtained by combining the calculated free energies of solid and liquid. We predict a temperature of  $6350 \pm 300$  K at the ICB, where the error quoted is the result of the combined statistical errors in the free energies of solid and liquid. Systematic errors due to the approximations of DFT are more difficult to estimate, and a definite value will only be obtained after the problem is explored with a more accurate implementation of quantum mechanics. We hope that quantum Monte Carlo techniques may serve this cause in the near future. However, it is possible to gauge *probable* errors by analysing the performance of the current techniques to describe known physical properties of iron. For example, a comparison of the dependence of the pressure of pure iron as a function of volume (a form of the *equation of state*) between our calculations and the experiments

shows a slight underestimation of the pressure (by 2-7% in the high-low pressure region respectively). An intuitive way to see how this error propagates in the melting curve, is to realise that on the melting line the actual pressure  $p$  is higher than the calculated one, and therefore the right melting curve is “shifted” to the right. This “corrected” melting curve is also shown in Fig. 2, as a dashed black line, and provides a prediction of the temperature at the ICB of about  $6200 \pm 300$  K.

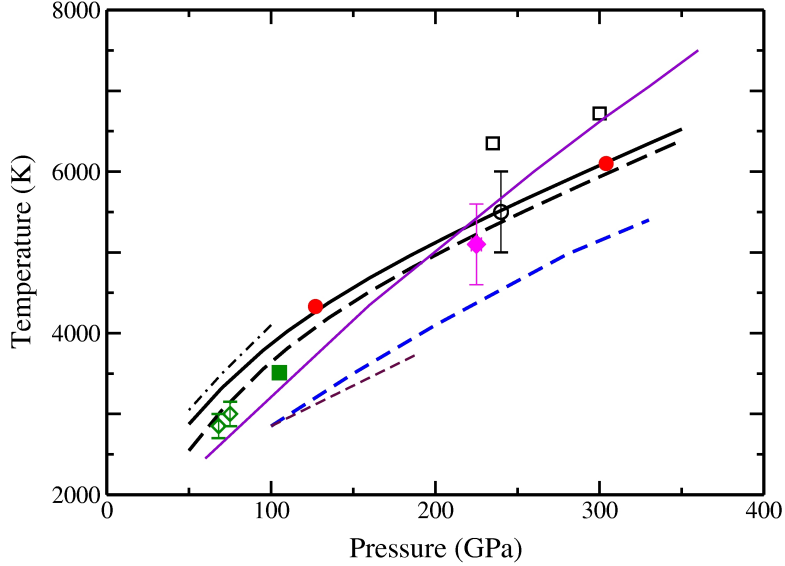


Figure 2: Comparison of melting curve of Fe from present calculations with previous experimental and *first principles* results: heavy solid and dashed curves: present work without and with pressure correction (see text); filled red circles: present corrected coexistence results (see text); blue dashed line: results of Laio et al. 2000; solid purple line : results of Belonoshko et al. 2000; black chained and dashed maroon curves: DAC measurements of Williams et al. 1987 and Boehler 1993 respectively; open green diamonds: DAC measurements of Shen et al. 1998; green filled square: DAC measurements of Ma et al. 2004; black open squares, black open circle and pink filled diamond: shock experiments of Yoo et al. 1993, Brown and McQueen 1986, and Nguyen and Holmes 2004. Error bars are those quoted in original references.

We also report on the same figure the theoretical results of Laio et al. (Laio et al. 2000) (dashed blue line) and Belonoshko et al. (Belonoshko et al. 2000) (solid purple line). These two groups used first principles in a different way. They used DFT calculations to fit some cleverly constructed model potential, and then used the model potential to calculate the melting curve using the technique of the “coexistence of phases”. In this technique, a large system containing solid and liquid is simulated using molecular dynamics. This “coexistence of phases” technique can be implemented in a number of different ways. For example, by constraining the pressure and the temperature to some chosen

values (NPT ensemble), the system always evolve towards a single phase, either solid or liquid, depending on whether the temperature is below or above the melting temperature for the chosen pressure. In this way it is possible to bracket the melting temperature. Other approaches include simulating the system in the NVE ensemble, where the volume and the total energy of the system are kept constant, or the NVT, NPH ensembles, where volume and temperature or pressure and enthalpy are kept constant respectively.

The method of the coexistence of phases and the one which relies on the explicit calculation of free energies are of course equivalent, if applied consistently. This was demonstrated recently for the calculation of the melting curve of aluminium, in which both methods were used in the context of first principles calculations and delivered the same results (Vočadlo and Alfè 2002, Alfè 2003). For the melting curve of iron however, the two methods cannot be directly compared, because the coexistence method was not employed directly in the context of DFT. Instead, a model potential was used for the coexistence simulations. This is the reason for the discrepancy between the melting curves of Laio et al. (Laio et al. 2000), Belonoshko et al. (Belonoshko et al. 2000), and ours (Alfè et al. 1999, 2002b). However, we showed that once the differences between DFT and the model potential are taken into account, it is possible to devise corrections which deliver exactly the same results (Alfè et al 2002c). To show this, in Fig. 2 we also report two melting points obtained by applying these corrections to the model potential of Belonoshko et al. (Belonoshko et al. 2000), which agree closely with the melting curve obtained from our free energy calculations.

Experimental results are also displayed on the figure for comparison. In the low pressure region we report the diamond anvil cell (DAC) experiments of Williams et al. (Williams et al. 1987), Boehler (Boehler 1993), Shen et al. (Shen et al. 1998) and the recent experiments of Ma et al. (Ma et al. 2004). Our “corrected” melting curve is in good agreement with the latter two more recent experiments. In the high pressure region only shock waves experiments are available. The measurements of Yoo at al. (Yoo et al. 1993) fall about 1000 K above our calculated melting curve, which is in good agreement with the results of Brown and McQueen (Brown and McQueen 1986) and the recent experiments of Nguyen and Holmes (Nguyen and Holmes 2004).

### **3.4 Constraints on the composition of the Earth’s core**

As mentioned above, the Earth’s core is mainly composed of iron, but the seismologically inferred density means that it must also contain some light impurities. The most popular candidates are sulphur, silicon, oxygen, carbon and hydrogen. The presence of these impurities modifies the melting temperature of the mixture with respect to that of pure iron. Moreover, the crystallisation of the inner core gives rise to compositional convection in the outer liquid core, and this convection helps to drive the geodynamo (Section 4). It is therefore also important to investigate what the

exact composition of the core is. Evidence from seismology indicates that at the ICB the density contrast between the solid and the liquid is between 4.5 % (Dziewonski and Anderson 1981, Masters and Shearer 1990, Shearer and Masters 1990) and 6 % (Masters and Gubbins 2003). This is much larger than that expected if the core were pure iron, and indicates a significant partitioning of light impurities between the solid and the liquid. This partitioning has been investigated by calculating the chemical potential of some of these light impurities in solid and liquid iron. At the ICB equilibrium between solid and liquid implies continuity of the chemical potential of both iron and a chosen light impurity: by imposing this continuity, it is possible to extract the equilibrium concentration of the chosen impurity in solid and liquid, and from this work out the density contrast. This strategy has been applied to sulphur, silicon and oxygen (Alfè et al. 2000, 2002d, 2002a, 2003). The results showed that sulphur and silicon demonstrate very little partitioning between solid and liquid iron, mainly because their size is very similar to the size of the iron atoms under ICB conditions. Conversely, oxygen partitioning is almost complete, with very little of it going into the solid inner core. This is intuitively explained by the fact that oxygen is significantly smaller than iron, and therefore would fit rather loosely in the solid. This waste of space results in an increase of its chemical potential, which tends to push it out into the liquid, where it can be accommodated much more efficiently.

Putting all this information together we ended up with a suggested composition for the inner core near the ICB which has about 8 % of sulphur/silicon and no oxygen in the inner core (we cannot distinguish between sulphur and silicon at this stage), and an outer core which contains about 8-10 % of sulphur/silicon plus 8-13 % of oxygen (the exact values depend on the exact value of the density contrast at the ICB, for which new estimates are still being published (Masters and Gubbins 2003)). This large partitioning of oxygen between the inner and the outer core is responsible to a large extent for the generation of the Earth's magnetic field (see below). The melting temperature of the mixture is reduced by  $\sim 800$  K with respect to that of pure iron due to this large partitioning of light impurities, so that our best estimate for the temperature of the ICB is  $\sim 5500$  K.

#### 4. Dynamo Models

The time-variable behaviour of the Earth's magnetic field, discussed above, shows that its source cannot be a permanent magnet; furthermore, the high interior temperatures of the Earth would prevent minerals from retaining any permanent magnetism. Instead, the Earth's magnetic field is maintained by a gigantic dynamo - the outer core. Motion of a fluid conductor in a magnetic field induces an electric current, and consequently a secondary magnetic field. Under the right circumstances, this field can reinforce the original magnetic field and lead to a "self-exciting" dynamo. The complicated motions generated by a rotating, convecting fluid such as the outer core are well-suited

to generating a dynamo. Furthermore, these fluid motions allow for both a slow drift, and a complete reversal, of the poles. However, although the basic theory has been understood for at least 80 years, the actual calculations are exceedingly challenging. As we discuss below, considerable progress has been made in modelling the behaviour of the dynamo in the last ten years; excellent summaries may be found in Busse (2000), Kono and Roberts (2002) and Glatzmaier (2002).

There are three reasons why numerical simulations of the core dynamo are more challenging than simulating the convecting mantle. Firstly, there are more governing equations to deal with. Modelling mantle convection requires solving two coupled differential equations: one describing the change in temperature due to fluid motion and diffusion of heat; and one describing the change in fluid velocity as a result of viscous and buoyancy forces. To model the dynamo, the effect of electromagnetic forces has to be added to the fluid motion, and an additional equation which links the change in magnetic field to fluid motion and magnetic diffusion is also required. Another way of viewing this same problem is mantle convection problem has only one characteristic timescale - that of thermal diffusion - but the core dynamo problem has three, wildly different, ones. These are the rotational period (1 day), the magnetic diffusion timescale ( $\sim 10^4$  years), and the viscous diffusion timescale ( $>1$  Gyr).

Secondly, the spatial resolution required is orders of magnitude higher for dynamo simulations than mantle convection models. The resolution required is set by the thickness of the fluid boundary layer, which for the core is determined mainly by the effective viscosity of the turbulently convecting material. Although this turbulent viscosity is much larger than the molecular viscosity of liquid iron (which is comparable to water), the likely boundary layer thickness is of order 0.1 km (Glatzmaier 2002). For comparison, typical boundary layer thicknesses for the mantle are of order 100 km. In practice, the kind of resolution required is not currently attainable, an issue we discuss further below.

Finally, the computational timestep is determined by the smaller of two transit times, those for the convecting material, and for propagating magnetic (Alfvén) waves. Mantle convection velocities are centimetres per year, while those of core convection are centimetres per second, and are similar to the Alfvén speed. As a result of the high core convective velocity, rotational effects (Coriolis forces) are important in the core while they can be neglected in the mantle. Because of the short transit times, timesteps in numerical dynamo calculations have to be much shorter than for mantle convection simulations. Typical dynamo simulations rarely last more than about 1 Myr (about 100 magnetic diffusion times), while 2D (though not 3D) mantle simulations can be run for the 4600 Myr age of the Earth (e.g. Nakagawa and Tackley 2004).

The limitations imposed on dynamo models by current computer technology are severe. For

instance, even with variable grid sizes, current models would need 10 times higher radial resolution to capture the turbulent boundary layer (Glatzmaier 2002). The corresponding increase in computer power required is unlikely to occur for at least a decade. As a result, the parameter space attainable with numerical models is a long way from that occupied by the real Earth. Current models have to either assume a core viscosity which is  $10^4$  times too large, or a rotation timescale which is  $10^4$  times too long (see Glatzmaier 2002). Perhaps surprisingly, despite these issues, several models have recently started to produce results which resemble the behaviour of the Earth's magnetic field.

As discussed above, the main characteristics of the Earth's magnetic field are its predominantly axial dipolar nature, its slow westwards drift, and its tendency to show excursions and complete reversals on  $\sim 0.1$  Myr timescales. The first two characteristics were relatively easy to obtain in numerical models. Figure 3 shows a comparison between the present-day Earth's magnetic field and a numerical simulation. The agreement is generally very good in terms of field intensity and geometry; models which are run for long enough also tend to generate a mean field aligned with the rotation axis (Kono and Roberts 2002). Figure 3 also makes the point that the short-wavelength structure in the core field is not visible at the surface, due to attenuation. Westwards drift has been obtained in many, though not all, models (Kono et al. 2000, Glatzmaier et al. 1999, Christensen and Olson 2003).

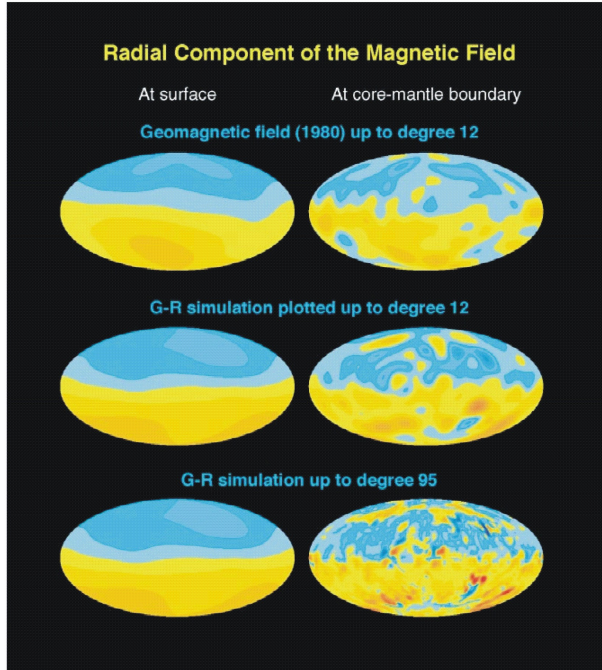


Figure 3: Comparison of observations and numerical models of the Earth's magnetic field at the surface (left side) and the CMB (right side), from Glatzmaier (2002). Top panel shows observations

for wavelengths  $>3300$  km; middle panel shows numerical results for same wavelength range; bottom panel shows results for wavelengths  $>400$  km. Note that the short-wavelength signals present at the CMB are not visible at the surface.

The last characteristic, polarity reversal, was much harder to obtain in numerical models, partly because of the very long computational times required, and partly because of worries that the results might be artefacts of the numerical procedures adopted, or initial transients (Ochi et al. 1999, Coe et al. 2000). Nonetheless, the first reversing dipoles were achieved in the mid 1990's (Glatzmaier and Roberts 1995, Kuang and Bloxham 1997) and can now be produced and studied routinely. Fig 4 compares a typical numerical result with a real record. Fig 4a is the numerical result: the bold line is the total field intensity, and the black and white boxes denote episodes of normal and reversed polarities. The total model time elapsed is just over 1 Myr (though an unrealistically slow Earth rotation is assumed). Fig 4b shows a time sequence (2.8 Myr duration) of the observed dipolar field intensity and polarity reversals. Although different in detail, the overall similarities of the two plots are evident: the frequency content and variability of the field intensities resemble each other, and the pattern of reversals are qualitatively similar.

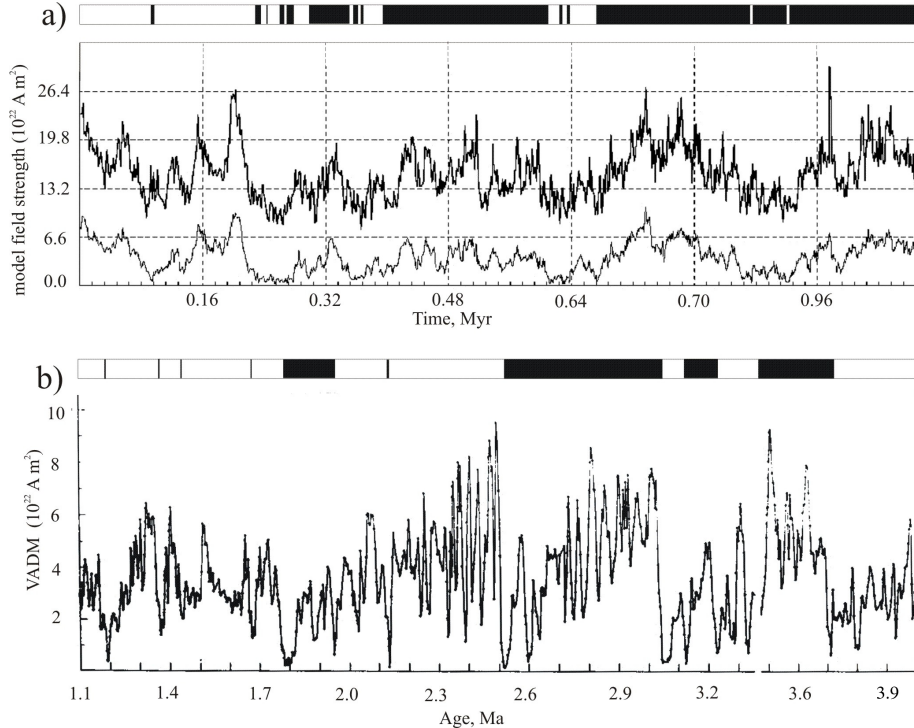


Figure 4: Time-variable behaviour of observed and modelled magnetic field. a) Model from Kutzner and Christensen (2002). Bold line is total magnetic field intensity, thin line is field due to dipole component alone. Black and white boxes show episodes of normal and reversed polarity (defined

by dipole angles of  $< 90^\circ$  and  $> 90^\circ$ , respectively). The magnetic diffusion timescale is 160 kyr. b) Observed recent field intensity variations and reversals based on sedimentary cores in the Pacific Ocean, from Valet and Meynardier (1993). "VADM" stands for virtual axial magnetic dipole.

Evidently, now that Earth-like dynamo behaviour is being routinely modelled, it is possible to discriminate between different models using quantitative (statistical) approaches (e.g. Dormy et al. 2000, McMillan et al. 2001, Coe et al. 2000). In doing so, further constraints on the physical processes governing dynamo behaviour will be obtained.

Fig. 5 shows one such discriminant. Fig. 5a is a histogram of the strength of the dipolar component of the field, showing that it is generally either strongly negative (S) or positive (N), and that neither orientation is preferred. Figs. 5b-d show the same data for three numerical models. Although each has different characteristics, none closely resembles the observations. Other discriminants, such as the frequency content of the magnetic field (Kono and Roberts 2002, Kutzner and Christensen 2002), and its time variability, may also be applied.

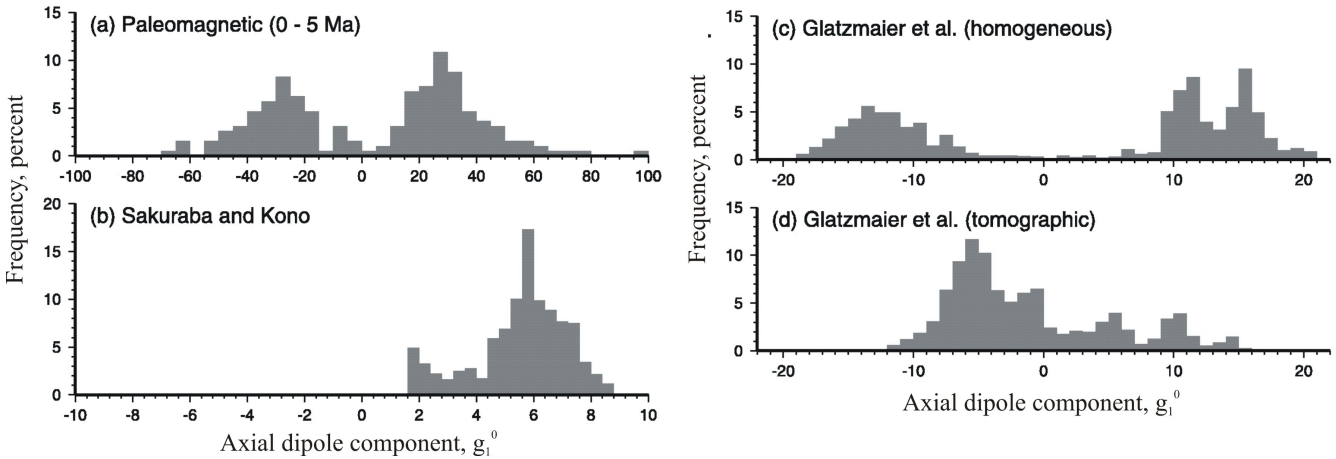


Figure 5: Comparison of observed frequency distribution of axial dipole component with numerical models, from Roberts and Kono (2002). a) Observed variation over last 5 Myr. The  $x$ -axis gives the strength of the dipole field and whether it is normal (positive) or reversed (negative). b) Similar plot from numerical model of Kono et al. (2000) over 50 kyr. Note that the field never reverses. c) As for b) but from Glatzmaier et al. (1999) with a homogeneous CMB heat flux and an interval of 0.3 Myr. d) As for c) but with a spatially varying core heat flux based on seismic observations.

A long-recognized consequence of the dynamo's existence is that the inner core might rotate relative to the outer core due to magnetic torques (e.g. Braginsky 1964). Seismological studies, making use of inner core anisotropy, subsequently appeared to confirm this hypothesis (Song and

Richards 1996, Su et al. 1996), though more recent observations have been more equivocal (Song 2003, Souriau and Poupinet 2003, Laske and Masters 1999). Similarly, the apparently preferred path taken during polarity reversals can be investigated with numerical models. Models with a core surface heat flux having a minimum in the Pacific showed preferential paths very similar to those inferred (Coe et al. 2000, Kutzner and Christensen 2004), though as noted above, the observations are disputed. The pattern of core heat flux may also influence the frequency of reversals (Glatzmaier et al. 1999). A particularly important example is the long ( $>30$  Myr) hiatuses in pole reversals, e.g. during the late Cretaceous and late Carboniferous-middle Permian. This kind of timescale is much longer than characteristic core timescales ( $O(10^4)$  yrs) and strongly suggests that the mantle is playing an important role (e.g. Hide 1967, Larson and Olson 1991), though the details have yet to be worked out. Similarly, the inner core is likely to have an effect on the frequency of magnetic reversals, though there is as yet no agreement on this point (Roberts and Glatzmaier 2001, Gubbins 1999, Sakuraba and Kono 1999).

As well as comparing them with observations, numerical models can also throw light on aspects of the geodynamo which are not observable at all. For instance, the toroidal component of the magnetic field is not directly observable (though see Jackson 2003), but may be at least equal in strength to the observable (poloidal) component. Similarly, numerical models may be able to place constraints on how much energy is dissipated by electromagnetic (Ohmic) heating in the core. This heating occurs mainly at short wavelengths, which are not observable at the surface. Understanding the energy requirements of the dynamo is critical to models of how the dynamo has evolved through time, and will be discussed further below.

At this point, it should again be stressed that the model parameters adopted are in some cases a factor of  $10^4$  different from those applicable to the Earth. The agreement between models and observations is thus somewhat surprising, and suggests that Earth-like dynamos are possible over a large parameter space. What is not yet clear is the extent to which the model results will change as more Earth-like parameters are approached. At this stage, a certain amount of caution needs to be exercised in interpreting numerical model results.

A relatively recent development, which avoids some of the problems inherent in the numerical models, is to simulate aspects of dynamo behaviour using laboratory experiments (Gailitis et al. 2003, Muller and Stieglitz 2002). While these experiments suffer from their own problems (e.g. the velocity field is generally specified *a priori* by the geometry of the experiment), they sample a different region of parameter space to the numerical models, and one in some ways closer to that of the Earth (Busse 2000). A powerful approach is to use laboratory experiments to verify extrapolations made from numerical models (Christensen and Tilgner 2004). It is likely that advances in

dynamo studies over the next decade will be driven increasingly by laboratory experiments as well as numerical models.

In summary, the last ten years have seen a breakthrough in dynamo studies. Although there remain caveats about the applicability of the parameter space explored, numerical models can now reproduce many aspects of the Earth's dynamo. Discriminating between different models of the basis of observations is likely to further constrain the physics of dynamo generation, for instance the roles of the mantle and inner core. The numerical models are likely to be increasingly complemented by laboratory studies.

## 5. The evolution of the core and dynamo

Given the understanding of dynamo generation provided by the models discussed above, it has become possible to investigate the long-term evolution of the dynamo. However, before examining this aspect, we will first discuss the manner in which it is powered at the present day.

### 5.1 Present-day heat balance

Although the distinction is not critical for the dynamo models discussed above, there are two sources of convective motion in the core: thermal convection, driven by core cooling and latent heat release (as the inner core solidifies); and compositional convection, which arises because the inner core as it freezes expels light elements (Section 3). Core solidification thus makes it easier to generate a dynamo, since the solidification provides additional sources of energy.

Whether or not convection occurs depends on the rate at which heat is extracted from the core into the mantle. In the absence of an inner core, convection only occurs if the CMB heat flux somewhere exceeds the adiabatic value, which is the maximum amount which can be transported without convection. It is therefore straightforward to predict whether or not a dynamo operates simply by tracking the CMB heat flux, or equivalently the core cooling rate (e.g. Nimmo and Stevenson 2000). However, if an inner core exists, a dynamo might operate even for a sub-adiabatic heat flux, due to the effect of compositional convection. In this situation, it is more convenient to use a criterion based on the rate of change of entropy, rather than energy (Gubbins et al. 2003, 2004). In this context, the entropy production rate can be thought of as the heat flux divided by a characteristic temperature, giving units of W/K. The entropy production rate also depends on a thermodynamic efficiency factor controlled by the location and temperature of heat sources and sinks. This efficiency factor shows that, for instance, compositional convection is a more efficient way of producing a dynamo than thermal convection. The utility of the entropy approach is that it allows both thermal and compositional effects to be accounted for. An important point is that almost all the entropy production terms are proportional to the rate at which the core is cooling. As a result, more rapid core cooling is more likely to allow a dynamo to operate. The entropy

requirement of a minimum core cooling rate, the equivalent of the adiabatic heat flux requirement, arises because the adiabatic entropy term is constant and negative; the positive terms (which arise from core cooling, latent heat release etc.) must outweigh this contribution.

A potentially important driving mechanism for the dynamo is radioactive decay of heat producing elements within the core. The entropy contribution in this case depends not on the core cooling rate, but on the rate of radioactive heat production. The most likely radioactive species to be present in the core is potassium-40, with a half life of 1.3 Gyr. Although early experimental results suggested that the partitioning of  $^{40}\text{K}$  into the core was negligible (Chabot and Drake 1999), more recent results (Gessmann and Wood 2002, Murthy et al. 2003, Lee et al. 2004) have found that significant partitioning is in fact likely to occur. The inferred abundance of potassium in the silicate mantle is slightly lower than elements (such as sodium) which have similar condensation temperatures (e.g. Lodders and Fegley 1998), suggesting that partitioning into the core is acceptable on geochemical grounds. Unfortunately, the uncertainties are large enough to preclude useful geochemical constraints. Nonetheless, it will be argued below that potassium is likely to have played a major role in the history of the geodynamo (Nimmo et al. 2004).

While calculating the rate of entropy production within the core is straightforward, the excess (positive) entropy required to drive the dynamo is unknown. The entropy production required depends on the amount of Ohmic dissipation in the core, which occurs at small ( $<100$  km) length scales. These length scales are not observable at the surface, because of upwards attenuation. Nor are such length scales readily achieved in simulations, for reasons discussed above. Finally, dissipation depends on both the toroidal and poloidal fields, only the latter of which can be observed. The excess entropy production rate required to drive the dynamo is probably of order 100 MW/K, equivalent to an Ohmic dissipation of about 0.5 TW (Buffett 2002, Gubbins et al. 2003, Roberts et al. 2003, Christensen and Tilgner 2004). Although there are large uncertainties in these values, the entropy production rate must exceed zero for a dynamo to operate.

In Section 3 above we argued that the various parameters describing the core's temperature structure and composition are reasonably well known. Given such a set of parameters, it is possible to calculate the various entropy production terms. Fig 6 shows the variation in these terms as a function of cooling rate for a set of core parameters appropriate to the present-day Earth. For a core which is not cooling, the only source of entropy is radioactive decay (generating 3 TW of heat in this example). The other positive entropy terms (latent heat release, compositional convection and core cooling) are all proportional to the cooling rate; added to the radioactive contribution, they make up the gross entropy production rate. The net rate, the amount available to drive the dynamo, is obtained by subtracting the (constant) adiabatic contribution. A cooling rate  $<6$  K/Gyr

(core heat flux of <5 TW) results in a negative net entropy contribution and, therefore, no dynamo. A higher core cooling rate generates a higher net entropy production rate; it also means that the inner core must have formed more recently. This is a tradeoff that we return to below.

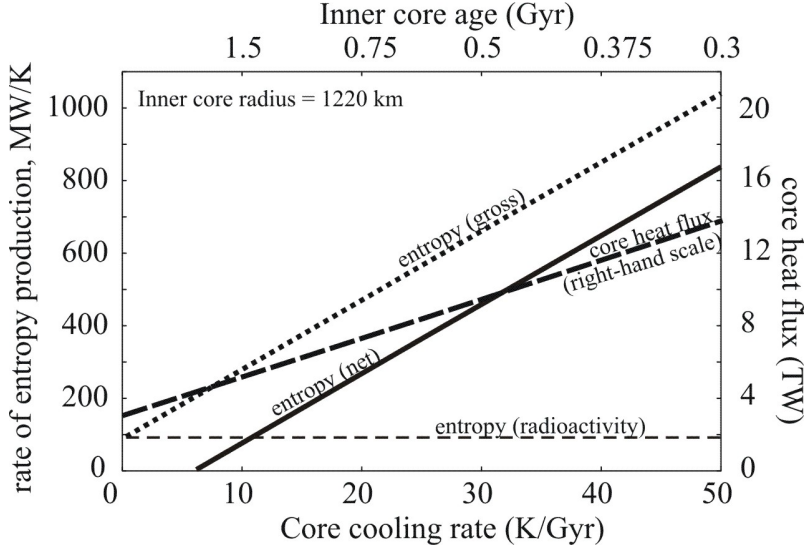


Figure 6: Variation in entropy production and heat flux with core cooling rate. Core temperature structure and parameters are from Nimmo et al. (2004); the core generates 3 TW of heat from radioactive decay. Gross entropy is the sum of all the positive entropy terms; net entropy has the adiabatic (constant, negative) contribution subtracted. The net entropy must exceed zero for a dynamo to be possible. The inner core age is calculated by assuming a constant cooling rate.

Figure 6 shows that the existence of a dynamo at the present day places constraints upon the rate at which the core is cooling. The rate of core cooling is determined by the ability of the mantle to remove heat. Importantly, independent estimates on this cooling rate exist, based on our understanding of mantle behaviour.

One approach to estimating the heat flux across the base of the mantle relies on the conduction of heat across the bottom boundary layer. The temperature at the bottom of this layer (the core) arises from extrapolating the temperature at the ICB outwards along an adiabat, and is about 4100 K (Fig. 1c). The temperature at the top of the layer is obtained from extrapolating the mantle potential temperature inwards along an adiabat, and is about 2700 K (Fig. 1c). The thickness of the bottom boundary layer, based on seismological observations, is 100-200 km. For likely lower mantle thermal conductivities, the resulting heat flux is probably in the range 6-12 TW (Buffett 2003). Values for the CMB heat flux based on the inferred contribution from rising convective plumes (Davies 1988, Sleep 1990) are a factor of 2-4 smaller, but are probably underestimates (Labrosse

2002, Bunge submitted). Figure 6 shows that a heat flux in the range 6-12 TW results in a net entropy production rate of 100-700 MW/K, likely enough to drive the dynamo.

The inferred value of the CMB heat flux has two implications. Firstly, it is a significant fraction of the heat flux at the Earth's surface, 42 TW (Slater et al. 1980). This result may help to explain the long-standing paradox that the mantle is getting rid of heat at about twice the rate at which it is being generated by radioactive decay (Breuer and Spohn 1993). Secondly, the inner core age implied by this heat flux (assumed constant) is young, about 0.6 Gyrs for the values assumed in Fig. 6. In practice, of course, the core heat flux will vary with time; investigating the time evolution of the core and mantle is the subject of the next section.

## 5.2 Thermal Evolution of the Earth

As discussed above, there is evidence that a dynamo similar to that at the present day has existed through the bulk of Earth history. It is therefore natural to enquire whether the prolonged life of the dynamo places constraints on the thermal evolution of the Earth. Anticipating the results of the sections below, it has recently become clear that the constraints are quite strong: generating a dynamo requires relatively rapid cooling of the core, while producing an inner core of the correct present-day size requires relatively slow core cooling (Buffett 2002, Gubbins et al. 2003). The parameter space which allows these two opposing constraints to be satisfied is relatively restricted, and in particular appears to require both a young inner core ( $<\approx 1.5$  Gyr) and significant ( $O(100$  ppm)) potassium in the core.

As discussed above, powering a dynamo requires the core cooling rate to exceed a given value. The core cooling rate depends on the rate at which the mantle extracts heat from the core. The ability of the mantle to extract heat depends, in turn, on the rate at which the mantle is cooling, and thus the behaviour of the near-surface boundary layer. Plate tectonics on the Earth is an efficient way of cooling the mantle; other planets, in which lateral motion of the surface material does not occur, probably cool much more slowly. This link, between the top 100 km of the Earth's mantle, and the behaviour of the dynamo, is both surprising and of fundamental importance. It also means that the evolution of the Earth as a whole has to be investigated in order to investigate the evolution of the core.

Modelling the thermal evolution of the Earth is a challenging problem. Although 3D numerical mantle convection models can be run, doing so for 4.5 Gyr is not yet possible. Alternatively, parameterized evolution schemes (e.g. Butler and Peltier 2000) can be adopted, which consider only globally-averaged properties and thus run very much faster, allowing a proper exploration of parameter space. The disadvantage of this approach is that complications, such as compositional layering or vertical viscosity variations, are less easy to include.

Figure 7 shows one such parameterized thermal evolution model, which generates a present-day thermal structure similar to Fig 1c while permitting a dynamo throughout Earth history. Fig 7a shows the temperature evolution of the core and mantle, and demonstrates the slow cooling regulated by radioactive decay in the mantle. The kink in the CMB temperature at 3.5 Gyr is due to the inner core starting to solidify. Fig 7b shows the evolution of the heat fluxes with time. The model present-day surface heat flux matches the observed value, and the CMB heat flux is 9 TW, in agreement with the arguments presented above. The core heat flux is high early on because of the presence of 400 ppm potassium, the effect of which is discussed below. Fig 7a also shows the net entropy production rate as a function of time, which is always positive, indicating a dynamo could have operated over the whole of Earth history. Fig 7b shows the inner core growth history, demonstrating that it is young (1.1 Gyr) and at the correct present-day size. The entropy production rate increases when the inner core solidifies, due to additional release of latent heat and compositional convection. Prior to inner core formation, the dynamo was maintained by the relatively rapid cooling rate of the core, plus radioactive decay.

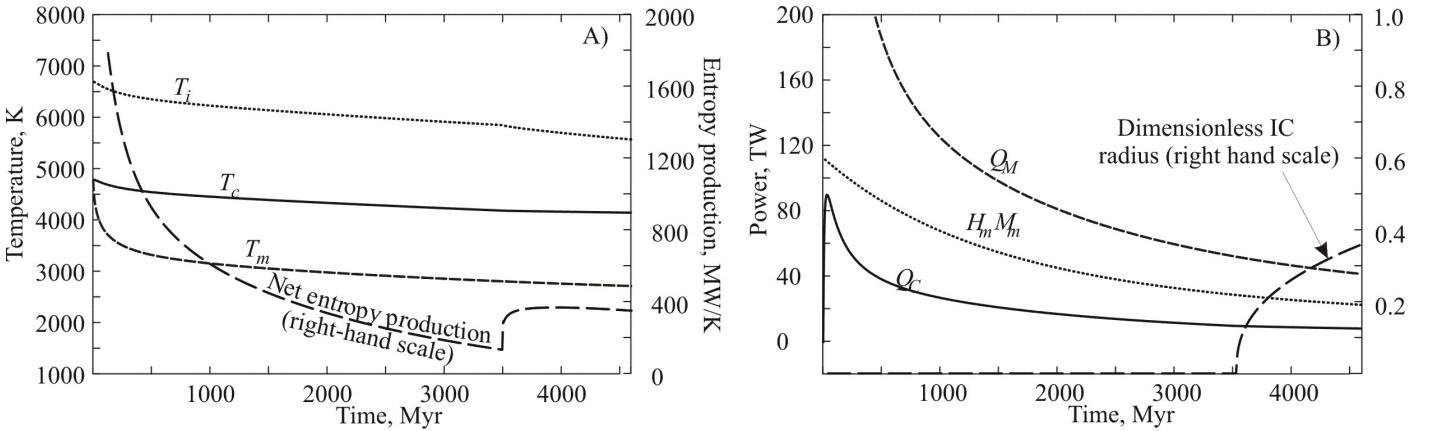


Figure 7: Parameterized thermal evolution model, reproduced from Nimmo et al. (2004), with 400 ppm potassium in the core. a) Temperature variation and entropy production rate as a function of time.  $T_m$  is the mantle temperature at the CMB,  $T_c$  is the core temperature at the CMB,  $T_i$  is the temperature at the centre of the planet, or at the ICB if an inner core exists. The kink in  $T_i$  at 3500 Myr is due to the onset of inner core solidification. b) Heat output and inner core size as a function of time.  $Q_M$  is the surface heat loss,  $H_m M_m$  the mantle contribution from radioactive decay and  $Q_C$  the core heat loss. The inner core size is normalized by the core radius.

The above model produces results compatible with our understanding of present-day Earth structure and geodynamo history. However, it does so mainly because of the presence of 400 ppm

potassium in the core. Similar models run without potassium generally result in an inner core which is much too large. This is because the heat released by the potassium reduces the rate at which the core cools and the inner core grows. In the absence of potassium, the core cooling rate has to be significantly reduced to generate an inner core of the correct present-day size. However, a lower core cooling rate and an absence of potassium means a reduction in the rate of entropy production (Fig. 6). There is thus a tradeoff between getting the correct inner core size (which requires slow cooling) and generating enough entropy to drive the dynamo (which requires rapid cooling).

This tradeoff is shown explicitly in Fig 8, which plots the mean entropy production rate against the present-day inner core size. Except at large inner core sizes, increasing the entropy production rate also results in a larger inner core. Adding potassium to the core shifts the curves to higher rates of entropy production for a given inner core size, because potassium both delays core solidification and is an additional entropy source. The curves demonstrate that none of the models lacking potassium are able to match both the entropy and the inner core size requirements simultaneously. It also turns out that none of the models with a correct present-day inner core size resulted in a core older than 1.5 Gyr.

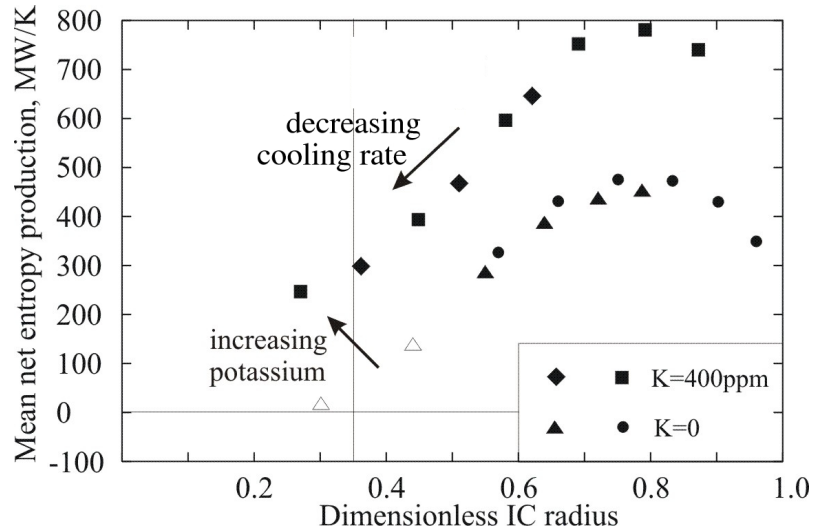


Figure 8: Tradeoff between time-averaged entropy production and present-day inner core (IC) size, normalized by core radius, from Nimmo et al. (2004). Open symbols have a minimum rate of entropy production  $<0$ , indicating an at least temporary cessation of the dynamo. Different points are for different mantle viscosity structures (and hence core cooling rates). Increased cooling rates lead to higher entropy production and larger IC sizes. Adding potassium (K) allows smaller inner cores for the same entropy production rate. Vertical line denotes present day IC size.

The results presented here depend on a large number of parameters, many of which are poorly known. Furthermore, as discussed above, the parameterized calculations are unlikely to capture

the full complexity of convection in the Earth. Nonetheless, the two main results - that the inner core is young, and that potassium is likely present in the core - are relatively robust. For instance, appealing to initially hotter core temperatures (rather than potassium) to delay inner core formation fails because the mantle is more efficient at cooling the core at higher temperatures.

Other authors have derived similar results using different techniques. For instance, Buffett (2002) found that obtaining an ancient inner core required a present-day heat flux across the CMB much lower than that inferred (Fig. 1c). To solve this problem he posited a significant amount of radioactive heat production, either within the bottom mantle boundary layer or in the core. Both Roberts et al. (2003) and Labrosse et al. (2001) examined the evolution of the core for specified CMB heat fluxes, and concluded that an inner core age of  $1 \pm 0.5$  Gyrs was most likely in the absence of any radiogenic heating.

In summary, whether or not a dynamo operates is ultimately controlled by the ability of the mantle to extract heat. There appears to be general agreement that both the present-day thermal structure of the Earth, and the maintenance of a dynamo, are compatible with a present-day CMB heat flux of about  $9 \pm 3$  TW (Buffett 2003, Labrosse and Macouin 2003, Nimmo et al. 2004). This heat flux implies an inner core age of  $<1.5$  Gyr. Parameterized thermal evolution models suggest that maintaining a dynamo over Earth history while producing an inner core of the correct size is difficult (Fig 8), because the dynamo requires rapid core cooling, while the small inner core requires slow core cooling. A likely resolution of this paradox, which is supported by experimental results, is the presence of O(100) ppm potassium in the core, generating 1.5-3 TW of radioactive heating at the present day.

## 6. Other Silicate Bodies

Although the bulk of this paper has focused on the Earth, many of the principles discussed can be applied equally well to other silicate bodies. In this section, we discuss some useful generalizations of the principles; describe briefly the data on cores of other planets; and suggest how these data might be interpreted. A useful summary of current understanding is in Stevenson (2003).

Figure 6 showed that sustaining a dynamo depends mainly on the rate of core cooling, and Section 5.2 argued that the core cooling rate is ultimately controlled by the rate at which the mantle can extract heat. The Earth is the only silicate body which currently exhibits plate tectonics; the other terrestrial planets do not have mobile plates, and as a result mantle cooling (and thus core cooling) is likely to be less rapid.

In the absence of an inner core, heat must be extracted at a rate exceeding the adiabatic core heat flux. This adiabat depends on gravity, and thus the size of the planet. However, the mantle's ability to extract heat also depends on gravity, though less strongly. This simple analysis suggests

that, other things being equal, it is easier to maintain dynamos in small bodies than larger ones at the same temperature. On the other hand, since larger bodies take longer to cool than small ones, and are likely to begin at higher temperatures, a dynamo (if present) is likely to persist for longer in a larger body. Of course, there are numerous additional complications, notably the increase in mantle viscosity (and decreasing mantle heat flux) with pressure, and the possible presence of an inner core. Nonetheless, this analysis suggests that a dynamo in a Moon- or Ganymede-sized body ( $g \approx 1 \text{ m s}^{-2}$ ) should be relatively easy to maintain, while mantle cooling on an Earth-sized body lacking plate tectonics is likely too sluggish to allow a dynamo to operate.

The role of gravity is also important because it controls the relative slopes of the core adiabat and melting curve. For the Earth, the adiabat is shallower than the melting curve (Fig. 1c); but for Mars, the two curves are roughly parallel (Williams and Nimmo 2004), and for even smaller bodies the adiabat may become steeper. Since the intersection of these curves determines the location of the inner core, it is clear that varying the gravity can have a dramatic effect on inner core behaviour.

The discussion of the Earth's dynamo showed that the role of contaminants in the core is important. In the solar system at large, the most significant contaminant is likely to be sulphur, which is both abundant and has a strong tendency to partition into iron at low pressures. Sulphur has two important effects. Firstly, at low pressures it can dramatically reduce the melting temperature of iron (Fei et al. 1997). Secondly, a core which is initially rich in sulphur (>21 wt%) will expel a dense fluid as it solidifies, which is the opposite case to that for the Earth's core. This behaviour is a consequence of the iron-sulphur phase diagram (Fei et al. 1997). The solidifying material will have a comparable density to that of the initial fluid (Kavner et al. 2001, Sanloup et al. 2002).

The effects of gravity and sulphur can be combined into a single diagram to generate four possible scenarios for the core (Fig. 9). The top left panel depicts the situation for Earth, where the adiabat is shallower than the melting curve, and the fluid expelled from the inner core is low density. The top right curve is similar, except here the fluid expelled from the inner core is high density (this situation applies to a sulphur-rich core). In this case, compositional convection will not occur, and the probability of generating a dynamo will be significantly reduced. The bottom left panel has an adiabat steeper than the melting curve, and a light fluid. Here core solidification will start at the outer core boundary. The solid core material is presumed to sink, re-melting as it does so and generating compositional convection; the fluid released during solidification will be stably stratified at the outer core boundary. Finally, the lower right panel shows a similar situation but with a dense fluid. In this case, both fluid and (re-melting) solid will tend to sink, generating vigorous convection.

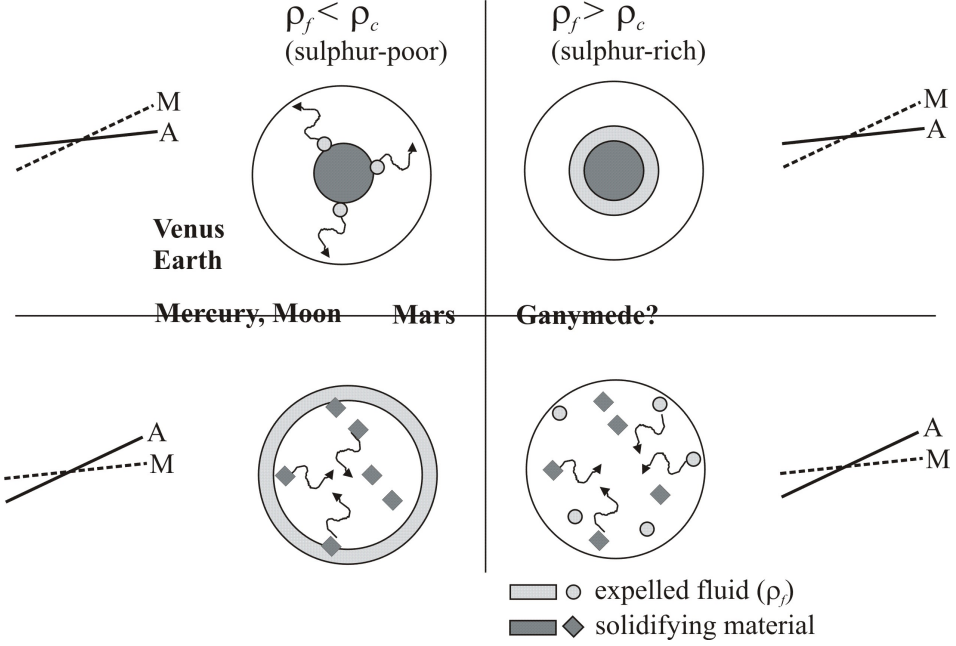


Figure 9: Different potential geodynamo regimes (see text). Labelled lines denote core melting curve (M) and adiabat (A). Fluid outer core and fluid released during core solidification have densities  $\rho_c$  and  $\rho_f$ , respectively. The case of  $\rho_c < \rho_f$  corresponds to a sulphur-rich scenario. For the sulphur-rich case we are assuming that the solid material is denser than the outer core fluid, which is uncertain.

It is clear that these different scenarios will have very different implications for core and dynamo evolution. Unfortunately, only one scenario has been studied in any detail. Although this scenario is likely appropriate to Earth and Venus, other bodies (especially Ganymede) may lie in quite different regimes.

### 6.1 Observations and Deductions

Figure 10 shows a selection of silicate bodies of interest. As explained in Section 2, density and moment of inertia data suggest that all possess cores, and tidal observations suggest that many have cores which are at least partially liquid. More interesting are the available magnetic observations. The Earth, Ganymede (Kivelson et al. 2002), Mercury (Connerney and Ness 1988) and possibly Io (Kivelson et al. 2001) have predominantly dipolar magnetic fields at the present day, which are likely the result of active dynamos. The Moon (Hood et al. 2001) and Mars (Acuna et al. 1999) do not have global fields now, but show local magnetic anomalies which are likely the result of an ancient dynamo. In the case of Mars, these crustal anomalies are enormous - an order of magnitude stronger than their terrestrial equivalents. Venus does not possess a global field (Russell 1980), and the surface temperatures are too high to retain magnetic anomalies.

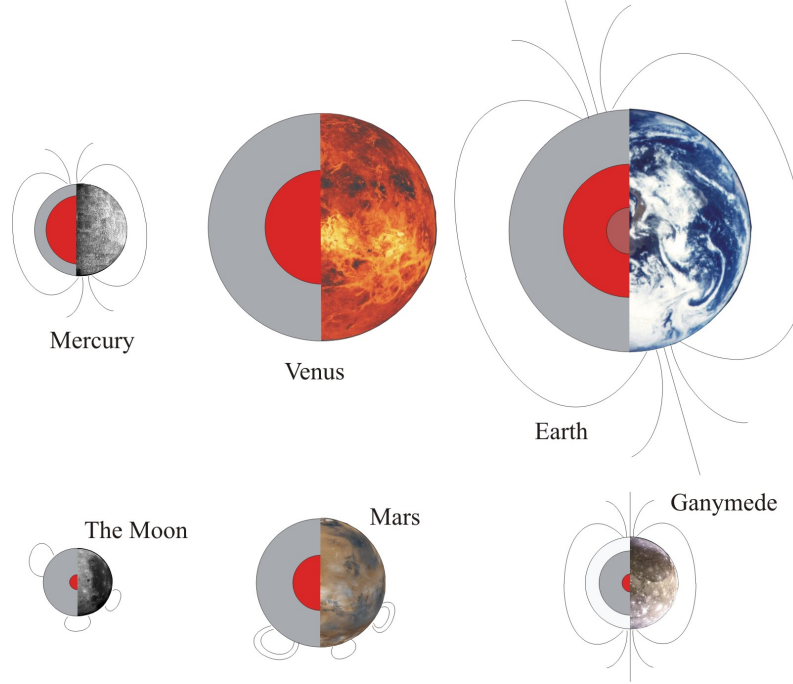


Figure 10: Illustration of internal structures and magnetic fields of silicate solar system bodies. Objects are drawn to scale; internal structures are based on information from Table 1. Magnetic fields are schematic, but reflect relative magnitudes and orientations.

How might these disparate observations be explained? The case of Venus is relatively straightforward: as suggested by the analysis above, an Earth-size planet which lacks plate tectonics is likely cooling too slowly to allow generation of a dynamo (Nimmo 2002). The ancient dynamo on Mars suggests early, rapid cooling; possible explanations for this are an early episode of plate tectonics (Nimmo and Stevenson 2000), overturn of an initially unstably stratified mantle (Elkins-Tanton et al. 2003), or an initially hot core (Williams and Nimmo 2004). With the exception of plate tectonics, similar arguments probably apply to the Moon (e.g. Stegman et al. 2003, Collinson 1993), although an alternative not requiring a dynamo is local magnetization by impact-generated plasmas (Hood and Huang 1991).

Mercury is more puzzling. It is not clear that a dynamo is the only way of generating its magnetic field (Schubert et al. 1988, Aharonson et al. 2004). If a dynamo is operating, it is hard to understand how: Mercury has been geologically inactive for 4 Gyr and must be cooling sluggishly at present (Hauck et al. 2004). Potassium is not an attractive explanation because it is probably too volatile to have been present when Mercury was forming; tidal heating may be an option but depends on very poorly known parameters (Schubert et al. 1988).

The dynamo of Ganymede is equally poorly understood. Firstly, Ganymede may be sulphur-rich, in which case it probably occupies a different regime of parameter space to the other terrestrial

planets (Fig. 9). Secondly, the strong background magnetic field of Jupiter may have important effects (Sarson et al. 1997). Thirdly, Ganymede's thermal evolution was probably drastically influenced by an episode of tidal heating midway through its history (Showman and Malhotra 1997), with consequences for the dynamo which remain obscure.

It is clear that our understanding of planetary dynamos remains rudimentary. This is in part due to the absence of data, especially time-resolved data, compared to the Earth. But it is also true that comparatively little theoretical effort has been devoted to understanding dynamos which may operate in quite different regimes from the familiar terrestrial one (Fig. 9). The acquisition of new data is likely to be a time-consuming and expensive process; it is to be hoped that swifter progress will be made in the theoretical understanding of planetary dynamos.

## 7. Conclusions

In the last decade, there have been three main advances in our understanding of the Earth's core and dynamo. Firstly, a combination of improved experimental and numerical techniques have allowed much tighter constraints to be placed on the density and melting behaviour of iron and iron compounds, and thus on the likely properties of the core. Secondly, numerical models generating realistic-looking dynamos have been achieved; these models make it possible to use the time-dependent behaviour of the Earth's magnetic field as a constraint on the behaviour of the core and mantle. Finally, the first two advances now allow the evolution of the core and dynamo to be investigated. Preliminary results suggest that the inner core is a young (<1.5 Gyr) feature, and that part of the energy driving the dynamo is provided by radioactive decay within the core.

The next decade is likely to see a change in emphasis. Despite the success of numerical models up to now, it is likely that future studies of both core properties and dynamo behaviour will be increasingly influenced by experimental results. As the crucial parameters become more tightly constrained, investigating the coupled core-mantle evolution problem will develop as a major area of interest. Observational constraints on the Earth's magnetic field are unlikely to improve significantly, but data on planetary magnetic fields will be dramatically expanded. The Messenger spacecraft will comprehensively characterize Mercury; the Dawn spacecraft will investigate the apparently magnetized asteroid Vesta; and sample return from both the Moon and Mars may take place. As the planetary observations improve, significant theoretical effort will need to be devoted to dynamos which may behave in very different ways to the Earth's. Thus, four centuries after the first publication in geomagnetism, this field shows no signs of dissipating.

## Acknowledgements

DA acknowledges support from the Royal Society and the Leverhulme Trust; FN the Royal Society and NSF-EAR 0309218. We thank Dave Gubbins for a careful review.

## References

- M.H. Acuna et al., *Science* **284**, 790, 1999.
- O. Aharonson et al., *Earth. Planet. Sci. Lett.* **218**, 261, 2004.
- D. Alfè, *Phys. Rev. B*, **68**, 064423, 2003.
- D. Alfè et al., *Nature*, **401**, 462, 1999.
- D. Alfè et al., *Nature*, **405**, 172, 2000.
- D. Alfè et al., *Phys. Rev. B*, **64**, 045123, 2001.
- D. Alfè et al., *J. Chem. Phys.*, **116**, 6170, 2002a.
- D. Alfè et al., *Phys. Rev. B*, **65**, 165118, 2002b.
- D. Alfè et al., *J. Chem. Phys.* **116**, 7127, 2002c.
- D. Alfè et al., *Earth Planet. Sci. Lett.*, **195**, 91, 2002d.
- D. Alfè et al., *Min. Mag.* **67**, 113, 2003.
- J.D. Anderson et al., *Nature* **384** 541, 1996.
- G. B. Bachelet et al., *Phys. Rev. B*, **26**, 4199, 1982.
- C.E. Barton, in *The Encyclopedia of Solid Earth Sciences*, D.K. James, ed., Van Nostrand Reinhold, New York, pp. 560, 1989.
- A. B. Belonoshko et al., *Phys. Rev. Lett.* **84**, 3638, 2000.
- J. Bloxham, *Nature* **405**, 63, 2000.
- R. Boehler, *Nature* **363**, 534, 1993.
- R. Boehler, *Rev. Geophys.* **38**, 221, 2000.
- S.I. Braginsky, *Geomag. Aeron.* **4**, 698, 1964.
- D. Breuer, T. Spohn, *Geophys. Res. Lett.* **20**, 1655, 1993.
- J. M. Brown and R. G. McQueen, *J. Geophys. Res.* **91**, 7485, 1986.
- B.A. Buffett, *Geophys. Res. Lett.* **29**, 2002.
- B.A. Buffett, *Science* **299**, 1675, 2003.
- F.H. Busse, *Ann. Rev. Fluid Mech.* **32**, 383, 2000.
- S.L. Butler, W.R. Peltier, *J. Geophys. Res.* **105**, 3175, 2000.
- N.L. Chabot, M.J. Drake, *Earth Planet. Sci. Lett.* **172**, 323, 1999.
- U.R. Christensen, P. Olson, *Phys. Earth Planet. Inter.* **138**, 39, 2003.
- U.R. Christensen, A. Tilgner, *Nature* **429**, 169, 2004.
- B.M. Clement, *Nature* **428**, 637, 2004.
- R.S. Coe et al., *Phil. Trans. R. Soc. Lond. A* **358**, 1141, 2000.
- D.W. Collinson, *Surv. Geophys.* **14**, 89, 1993.

J.E.P. Connerney, N.F. Ness, in *Mercury*, F. Vilas et al., eds., pp.494, Univ. Ariz. Press, Tucson, 1988.

G.F. Davies, *J. Geophys. Res.* **93** 10467, 1988.

E. Dormy et al., *Geochem. Geophys. Geosyst.* **1** 2000GC000062, 2000.

R.M. Dreizler and E.K.U. Gross, *Density Functional Theory*, Springer-Verlag, 1990.

D.J. Dunlop and Y. Yu, in *Geophys. Monogr.* 145, J.E.T. Channell et al., eds., pp. 85, Amer. Geophys. Union, 2004.

A.M. Dziewonksi, D.L. Anderson, *Phys. Earth Planet. Inter.* **25**, 297, 1981.

L.T. Elkins-Tanton et al., *Meteorit. Planet. Sci.* **38**, 1753, 2003.

Y. Fei et al., *Science* **275**, 1621, 1997.

D. Frenkel, and B. Smit, *Understanding Molecular Simulation* (Academic Press, 1996).

A. Gailitis et al., *Surv. Geophys.* **24**, 247, 2003.

C.K. Gessman, B.J. Wood, *Earth Planet. Sci. Lett.* **200**, 63, 2002.

G.A. Glatzmaier, P.H. Roberts, *Nature* **377**, 203, 1995.

G.A. Glatzmaier et al., *Nature* **401**, 885, 1999.

G.A. Glatzmaier, *Ann. Rev. Earth Planet. Sci.* **30**, 237, 2002.

D. Gubbins, *Geophys. J. Int.* **137**, F1, 1999.

D. Gubbins et al., *Geophys. J. Int.* **155**, 609, 2003.

D. Gubbins et al., *Geophys. J. Int.* **157**, 1407, 2004.

S.A. Hauck et al., *Earth Planet. Sci. Lett.* **222**, 713, 2004.

R. Hide, *Science*, **157**, 55, 1967.

P. Hohenberg, and W. Kohn, *Phys. Rev.* **136**, B864, 1964.

L.L. Hood et al., *J. Geophys. Res.* **106**, 27825, 2001.

L.L. Hood, Z. Huang, *J. Geophys. Res.* **96**, 9837, 1991.

J.A. Jacobs, *Surv. Geophys.* **19**, 139, 1998.

A. Jackson, *Nature* **424**, 760, 2003.

H. Jeffreys, *The Earth*, Cambridge Univ. Press, 1929.

A. Kavner et al., *Earth Planet. Sci. Lett.* **185**, 25, 2001.

A. Khan et al., *J. Geophys. Res.* **109**, E09007, 2004.

M.G. Kivelson et al., *J. Geophys. Res.* **106**, 26121, 2001.

M.G. Kivelson et al., *Icarus* **157**, 507, 2002.

W. Kohn and L. Sham, *Phys. Rev.* **140**, A1133, 1965.

M. Kono et al., *Philos. Trans. R. Soc. Lond. A* **358**, 1123, 2000.

M. Kono, P.H. Roberts, *Rev. Geophys.* **40**, 2002.

- A.S. Konopliv, C.F. Yoder, *Geophys. Res. Lett.* **23**, 1857, 1996.
- W. Kuang, J. Bloxham, *Nature* **398**, 371, 1997.
- C. Kutzner, U.R. Christensen, *Phys. Earth Planet. Inter.* **131**, 29, 2002.
- C. Kutzner, U.R. Christensen, *Geophys. J. Int.* **157**, 1105, 2004.
- S. Labrosse et al., *Earth Planet. Sci. Lett.* **190**, 111, 2001.
- S. Labrosse, *Earth Planet. Sci. Lett.* **199**, 147, 2002.
- S. Labrosse, M. Macouin, *Comptes Rendus Geosc.* **335**, 37, 2003.
- A. Laio et al., *Science* **287**, 1027, 2000.
- C. Laj et al., *Nature* **351**, 447, 1991.
- R.L. Larson, P. Olson, *Earth Planet. Sci. Lett.* **107**, 437, 1991.
- G. Laske, G. Masters, *Nature* **402**, 66, 1999.
- P.W. Layer et al., *Science* **273**, 943, 1996.
- K.K.M. Lee et al., *Geophys. Res. Lett.* **31**, L11603, 2004.
- K. Lodders, B. Fegley, *The Planetary Scientist's Companion*, Oxford Univ. Press, 1998.
- J.J. Love, *Geophys. J. Int.* **140**, 211, 2000.
- Y. Ma et al., *Phys. Earth Planet. Int.*, **143-144**, 455, 2004.
- T. G. Masters, D. Gubbins, *Phys. Earth Planet. Inter.* **140**, 159, 2003.
- T. G. Masters and P. M. Shearer, *J. Geophys. Res.* **95**, 21691, 1990.
- M.W. McElhinny, W.E. Senanayake, *J. Geophys. Res.* **85**, 3523, 1980.
- D.P. McKenzie, M.J. Bickle, *J. Petrol.* **86**, 625, 1988.
- D.G. McMillan, *Geochem. Geophys. Geosyst.* **2**, 2000GC000130, 2001.
- J. Margot et al., *Eos Trans. AGU* **85**(47), abs. G33A-02, 2004.
- R. Montelli et al., *Science* **303**, 338, 2004.
- U. Muller, R. Stieglitz, *Nonlinear Processes Geophys.* **9**, 165, 2002.
- C.D. Murray, S.F. Dermott, *Solar System Dynamics*, Cambridge Univ. Press, 1999.
- V.R. Murthy et al., *Nature* **323**, 163, 2003.
- T. Nakagawa, P.J. Tackley, *Earth Planet. Sci. Lett.* **220**, 107, 2004.
- J. H. Nguyen and N. C. Holmes, *Nature*, **427**, 339, 2004.
- F. Nimmo, *Geology* **30**, 987, 2002.
- F. Nimmo et al., *Geophys. J. Int.* **156**, 363, 2004.
- F. Nimmo, D. Stevenson, *J. Geophys. Res.* **105**, 11969, 2000.
- M.M. Ochi et al., *Phys. Plasmas* **6**, 777, 1999.
- A.R. Oganov, S. Ono, *Nature* **430**, 445, 2004.

R.G. Parr and W. Yang *Density-Functional Theory of Atoms and Molecules*, Oxford Science Publications, 1989.

- J. P. Perdew, K. Burke, Matthias Ernzerhof, *Phys. Rev. Lett.* **77**, 3865, 1996.
- M. Prevot and P. Camps, *Nature* **366**, 53, 1993.
- P.H. Roberts, G.A. Glatzmaier, *Geophys. Astrophys. Fluid Dyn.* **94** 47, 2001.
- P.H. Roberts et al., in *Earth's core and lower mantle*, C.A. Jones et al., eds., Taylor & Francis, 2003.
- C.T. Russell, *Rev. Geophys.* **18**, 77, 1980.
- C. Sanloup et al., *J. Geophys. Res.* **107**, 2272, 2002.
- G.R. Sarson et al., *Science* **276**, 1106, 1997.
- A. Sakuraba, M. Kono, *Phys. Earth Planet. Inter.* **111** 105, 1999.
- G. Schubert et al., in *Mercury*, pp. 429, eds. F. Vilas et al., Univ. Ariz. Press, 1988
- J.G. Sclater et al., *Rev. Geophys. Space Phys.* **18**, 269, 1980.
- P. M. Shearer and T. G. Masters, The density and shear velocity contrast at the inner core boundary, *Geophys. J. Int.* **102**, 491, 1990.
- G. Shen et al., *Geophys. Res. Lett.* **25**, 373, 1998.
- A.P. Showman, R. Malhotra, *Icarus* **127**, 93, 1997.
- N.H. Sleep, *J. Geophys. Res.* **95**, 6715, 1990.
- X. Song, P.G. Richards, *Nature* **382**, 221, 1996.
- X. Song, Earth's Core, Geodynamics Series 31, Amer. Geophys. Union, 45, 2003.
- A. Souriau, G. Poupinet, Earth's Core, Geodynamics Series 31, Amer. Geophys. Union, 65, 2003.
- D.R. Stegman et al., *Nature* **421**, 143-146, 2003.
- S. Stein, M. Wysession, *Seismology*, Blackwell Publishers, 2000.
- D.J. Stevenson, in *Origin of the Earth*, 231-250, H.E. Newsom and J.E. Jones, eds., Oxford Univ. Press, 1990.
- D.J. Stevenson, *Earth Planet. Sci. Lett.* **208**, 1, 2003.
- W.J. Su et al., *Science* **274**, 1883, 1996.
- W.B. Tonks, H.J. Melosh, *J. Geophys. Res.* **98** 5319, 1993.
- J.-P. Valet, L. Meynadier, *Nature* **366**, 234, 1993.
- J.-P. Valet, *Rev. Geophys.* **41**, 1004, 2003.
- L. Vočadlo and D. Alfè, *Phys. Rev. B*, **65**, 214105, 2002.
- Y. Wang and J. Perdew, *Phys. Rev. B* **44**, 13298, 1991.
- J.G. Williams et al., *J. Geophys. Res.* **106**, 27933, 2001.

- J.-P. Williams, F. Nimmo, *Geology* **32**, 97, 2004.
- Q. Williams et al., *Science* **286**, 181, 1987.
- Q. Williams, E.J. Garnero, *Science* **273**, 1528, 1996.
- C.F. Yoder et al., *Science* **300**, 299, 2003.
- C. S. Yoo et al., *Phys. Rev. Lett.* **70**, 3931, 1993.